Nuclear Materials and Energy 28 (2021) 101029

Contents lists available at ScienceDirect

Nuclear Materials and Energy

journal homepage: www.elsevier.com/locate/nme

Assessment of laser induced breakdown spectroscopy accuracy for determination of hydrogen accumulation in tungsten

E.D. Marenkov [a,*], I.P. Tsygvintsev [b], Yu.M. Gasparyan [a], A.A. Stepanenko [a]

[a] National Research Nuclear University MEPhI (Moscow Engineering Physics Institute), Kashirskoe Shosse, 31, Moscow 115409, Russia
[b] Keldysh Institute of Applied Mathematics, Miusskaya Square, 4, Moscow 125047, Russia

ARTICLE INFO

Keywords:
LIBS
Saha-Boltzmann
Retention
Hydrogen
Plasma-facing components

ABSTRACT

Laser-induced breakdown spectroscopy (LIBS) is an in situ method of determining hydrogen (H) content in plasma-facing materials in tokamak fusion reactors. Observing radiation from the plasma plume produced by a powerful laser pulse during the target exposition characterizes the sample composition. This is typically accomplished using the Saha-Boltzmann (SB) plot technique under local thermodynamic equilibrium (LTE) conditions. Despite many experimental studies dedicated to applying LIBS to determine H isotope retention in fusion reactor materials, the current understanding of this method's intrinsic accuracy remains inadequate. In this report, we use numerical calculations to estimate the relative error of determining H content in a sample using LIBS. As an example. we consider LIBS to study a W sample loaded with H in a vacuum. Under typical LIBS pulse parameters (10^9 W/cm^2 and 12 ns duration), the error can be quite large, approximately 70%. We demonstrate that the error tends to decrease as the laser pulse intensity increases. Various factors contributing to the relative error are examined and their dependence on the LIBS plasma parameters is discussed. The SB plot remains a straight line even when LTE conditions are violated, making it difficult to anticipate the experimental results' error.

1. Introduction

The development of various in situ measurement methods of hydrogen isotope accumulation in first wall materials and divertor targets is important for controlling hydrogen isotope retention in components of future fusion tokamaks including the ITER Project [1,2]. Laser-induced breakdown spectroscopy (LIBS) can be used for this task [3–6]. In LIBS, a spot on a surface of interest is irradiated by a powerful laser pulse. In tokamaks, LIBS is often conducted without the main plasma in ultrahigh vacuum conditions, although LIBS can also be used under atmospheric pressures. The composition of the ablated plasma material is then determined spectroscopically, providing information about the sample [7].

The LIBS plasma density is typically high ($>10^{17}$ cm^{-3}) and it is supposed that local thermodynamic equilibrium (LTE) in the plume is valid [8,9]. Due to strong line broadening, plasma is optically transparent in the lines of interest. A Saha-Boltzmann (SB) plot can be used to determine the plasma temperature and total number of radiating particles [10–12]. If hydrogen (H) lines are observed, it is straightforward in principle to determine the plasma plume's H content. The SB plot also assesses the plume's total number of radiating particles (H atoms), which is necessary for H retention characterization.

Dedicated experiments showed that this method is suitable for analyzing relevant fusion samples [6,13–15]. Several studies compared LIBS to other H retention characterization methods. For example, deuterium depth profiles in W-Al and Be-W compounds were obtained using LIBS measurements in [16–18] and compared to secondary ion mass spectroscopy (SIMS) results. Similar measurements were reported in [19,20] for lithiated W samples. In general, good qualitative and sometimes quantitative agreement between SIMS and LIBS was demonstrated, despite typically large scatter of W line intensities in SB plots [16–18] that were likely associated with the radiation absorption. Paris et al. [21] also used LIBS and SIMS to measure the depth profiles of various elements in ASDEX Upgrade tokamak tiles, but their LIBS and SIMS D profiles in some cases differed by orders of magnitude. Nuclear reaction analysis (NRA), thermal desorption spectroscopy (TDS), and LIBS methods were employed in [22] to analyze D retention in W samples. Predictably, NRA and TDS showed practically the same D retention, while the LIBS results were off by almost 100 times. Comparing D retention obtained by TDS and LIBS in WBe co-deposits

* Corresponding author.
E-mail address: edmarenkov@mephi.ru (E.D. Marenkov).

https://doi.org/10.1016/j.nme.2021.101029
Received 18 February 2021; Received in revised form 17 May 2021; Accepted 18 May 2021
Available online 24 May 2021

[23] showed practically the same D concentration, although the SB plot contained only one D line and the plume temperature was determined from the W and Be line intensities.

Thus, there is no reliable overall understanding of LIBS accuracy for determining H content. However, this factor is very important for ITER, in which "order of magnitude" estimates of H isotope content in plasma-facing components are not enough and accuracy on the order of 20% in measurements is required [24,25]. Therefore, it is necessary to better understand the intrinsic accuracy of spectroscopical measurements applying LIBS for fusion, in particular the Saha-Boltzmann (SB) plot technique.

In this study, we assess the contribution of various factors to this method's precision. We numerically calculated a plasma plume's dynamics during and after laser pulse impact. Then we tried to "restore" the plume's H content at different times using the SB method and compared the results with nominal values determined by the calculations. We used tungsten (W) as the sample material since the ITER divertor's targets were made from it. Only LIBS under vacuum conditions was considered.

2. Model setup

2.1. Plume expansion hydrodynamics

Plume formation dynamics and expansion in a vacuum were simulated using the one-fluid hydrodynamics code 3DLINE [26]. The code was previously used to model laser interactions with solids [27–29] and demonstrated a good agreement with experiments. Laser absorption in the plasma and sample (in our case W) is described using a hybrid model that combines the geometrical-optics ray-tracing method with the one-dimensional (1D) solution of the Helmholtz wave equation in regions where the geometrical optics are inapplicable [30]. Inverse Bremsstrahlung absorption is supposed to be the main mechanism of laser energy deposition in plasma. Collisional-radiative equations are used to determine the W distribution over ionized and excited states [31]. Solid-to-plasma transitions are described by an equation of state obtained via the FEOS method [32,33] without accounting for metastable states at liquid–gas phase transitions. This approximation adequately estimates the target's integral ablated mass [34].

Because the 3DLINE model includes only one fluid, it is impossible to simulate W and H dynamics separately. Instead, we assume that W and H move simultaneously, and the total H density (that is, the sum of the H and H^+ densities) is a fixed fraction of the total W (both neutral and ion) density corresponding to a typical value of retained H in W of 1%, $n[H] = 0.01\, n[W]$ [35,36]. Simultaneous movement of the H and W fluids is justified by an estimation of the drag force between W^+ and H^+ ions which indicates that there should be no significant separation between them. Indeed, at T ~ 1 eV and n[W^+] ~ 10^{17} cm^{-3}, the momentum transfer time scale $\tau_{WH} = \frac{3(2\pi)^{3/2}T^{3/2}\sqrt{m_H}}{n[W^+]\, e^4 ln\Lambda} \sim 3{\cdot}10^{-12}$ s. This time is much shorter than the characteristic plume expansion time estimated via the simulations, which is on the order of 30 ns. Therefore, W-H ion separation can indeed be neglected. The simulations show that the H and W are rapidly ionized during the laser pulse, and the degree of W ionization is constantly high. However, the H is slowly neutralized and, in principle, the drag force between neutral H atoms and charged W fluids is lower. Nevertheless, at the beginning, since the H ions gain the same momentum as the W ions due to strong friction between them, the H atoms will keep up with the W atoms due to inertia.

2.2. Radiation transport model

After the plume density and temperature are calculated, the radiation transport problem is solved using the modified RADTRANSP code developed for radiation transport calculations in quasi-1D geometry. RADTRANSP was recently benchmarked with a widely used Monte Carlo code EIRENE [37]. A detailed description of the code's equations is provided in [38]. The code was modified for this study: recombination and ionization processes necessary to describe LTE transitions were added. The density of hydrogen atoms n_j [cm^{-3}] in excited state j is given by the following equation:

$$\frac{dn_j}{dt} \equiv -n_j\left(\sum_{k<j}A_{jk} + n_e\sum_{k\neq j}C_{jk} + \sum_{k\neq j}B_{jk}\widetilde{I}_{jk} + S_j n_e\right) + R_j n_e^2 n_{ion} + \sum_{k>j}n_k\left(A_{kj} + n_e C_{kj} + B_{kj}\widetilde{I}_{kj}\right) + \sum_{k<j}n_k\left(n_e C_{kj} + B_{kj}\widetilde{I}_{kj}\right) = 0 \quad (1)$$

where A and B are the Einstein coefficients, S_j is the electron impact ionization rate from level j, R_j is the three-body recombination rate, C is the electron impact excitation/deexcitation rate, and $\widetilde{I}_{jk}$ is the radiance averaged over a solid angle corresponding to j-k transitions. Dielectronic and radiative recombination are not taken into account because in low-T and high-density plasmas, the three-body recombination dominates.

Equation is combined with the spectral radiance equations $I(\omega, \mathbf{\Omega})$. If the total density of radiating particles $\overline{n} = n_{ion} + \sum_j n_j$ and electrons n_e is given, the system of equations can be solved to find the radiation field I, the H ion (or proton) density $n_{ion} \equiv n[H^+]$, and the distribution of atoms over excited states $n_j[H]$. Since the first W ionization potential (7 eV) is lower than that of H (13.6 eV), and the H density is much lower than that of W from the beginning, most of the electrons are provided by W ionization, $n_e >> n_{ion}^H$, so we can assume that n_e is a given quantity and solve our equations to find H densities n_j and n_{ion}^H and the radiation intensities.

The RADTRANSP code uses a quasi-1D geometry, meaning that all of the densities depend only on one coordinate × , while the radiance is a function of × and ray direction $\mathbf{\Omega}$. This approximation works for planar geometry when the radiation transport is considered in a non-uniform plasma slab. Because the plasma plume has an almost spherical shape, we restrict the radiation transport direction to a narrow cone around the line of sight, basically using a known backward-forward approach for radiation transport problems.

In a non-uniform plasma line profile, the shape variation plays an important role as it may lead to preferential radiation transport in certain directions. We calculate the line profiles taking into account the Doppler and Stark effects [38]. In our case the very high-density Stark effect strongly dominates. The Einstein coefficients, collision rate C, and ionization rate S of H were taken from ADAS [39].

Complete thermodynamic equilibrium is established if the plasma is opaque in all radiation. Then the radiance I is given by the Planck black body formula, and the terms containing Einstein coefficients A and B in Equation are canceled out [40]. The sum of the remaining terms is zero if the population of excited states n_j follows the Boltzmann distribution and $R_j n_e^2 n_{ion} = S_j n_e$. The last equivalence can be used to determine the three-body recombination rate R_j and is therefore always satisfied.

Local thermodynamic equilibrium (LTE) conditions can be derived directly from Equation . If the plasma is transparent in a line j-k, the densities $n_{j,k}$ have equilibrium Boltzmann values if $A_{jk} << C_{jk} n_e$. Indeed, as the line is transparent, $\widetilde{I}$ can be neglected compared to the spontaneous emission terms, and we again use the same equations as in the previous case of complete equilibrium. The criterion $n_e >> A_{jk}/C_{jk}$ therefore follows as demonstrated in [41,42].

2.3. Saha-Boltzmann plot

If the line emission due to a j-k transition is fully transparent, its radiance is:

$$I_{jk} = \frac{E_{jk}}{4\pi}A_{jk}\int n_j\, ds\, d\Omega \quad (2)$$

where ds denotes integration along a chosen ray and $d\Omega$ represents integration over all of the rays detected by the spectrometer. E_{jk} is the transition energy. The level abundances n_j are given by the Boltzmann distribution:

$$n_j = \frac{n_a g_j}{Z(T_e)} exp\left(- \frac{E_j}{T_e}\right) \quad (3)$$

where Z is the partition function. Equation yields:

$$L \equiv \frac{4\pi I_{jk}}{A_{jk} E_{jk} g_j} = \int \frac{n_a}{Z(T_e)} exp\left(- \frac{E_j}{T_e}\right) ds\, d\Omega \quad (4)$$

where $n_a = \sum n_j$ is the total density of the emitting particles. If T_e does not depend on s, Equation reduces to:

$$lnL = -\frac{E_j}{T_e} + ln\frac{N_a}{Z} \quad (5)$$

Therefore, the dependence of lnL on E_j is linear. Intensities I_{jk} are obtained experimentally, then T_e and $N_a = \int n_a ds\, d\Omega$ can be found using Equation . This technique is usually called a Saha-Boltzmann plot and is used to interpret calibration-free LIBS experiments. If the spectrometer registers all of the radiation emitted from the plasma plume, N_a is the total number of radiation particles in the plasma, for example, H atoms. At a sufficiently low T_e, the H ionization degree is also low and N_a equals the total number of H atoms in the ablated spot.

This approach's main limitations are as follows. First, it is valid only for fully transparent lines as the intensities of opaque lines do not satisfy Equation and the corresponding points should not be considered in the Saha-Boltzmann plot. Second, if the plume plasma is non-uniform, T_e depends on s, and integrating Equation cannot be carried out separately for n_a, so the dependence of $\ln L$ on E_j will not be linear. Third, the H degree of ionization is low at a low T_e, but the radiation intensity is also lower at a small T_e, and thus it may be difficult to register the radiation at necessary times. We consider the effect of these factors on the LIBS results' accuracy and estimate the SB method's corresponding precision.

The influence of plasma non-homogeneity on the SB plot can be better understood if one considers the model situation with $n_a = n_1 exp(-\beta s)$ and $T = 1/(C - \alpha s)$, where α, β, and C are the profile's parameters. The partition function for H $Z = 1$ and does not depend on T_e. In this case, integration in Equation can be carried out along a line of sight $0 < s < R$ to obtain:

$$L = \frac{N_a}{Z} exp\left(- E_j C\right) \frac{exp\left(\left[E_j\alpha - \beta \right] R\right) - 1}{\left[E_j\alpha - \beta \right] R} \quad (6)$$

If $\left[E_j\alpha - \beta \right] R << 1$, the fraction ≈ 1 does not depend on E_j, L preserves an exponential dependence on E_j, and SB plot remains a straight line. The last condition can be recast in a more general form: $R\frac{E_j}{T_e}\frac{dlnT_e}{ds} << 1 + R\frac{dlnn_a}{ds}$ (7)

suggesting that for the SB plot to remain a straight line, the electron temperature should be sufficiently slow and/or n_a must change sufficiently fast.

3. Results and discussion

3.1. Test RADTRANSP calculations

We start by testing the radiation transport calculations in a uniform plasma slab. The following cases are considered: 1) a fully transparent 50 μm thick plasma with an electron density $n_e = 10^{18}$, 10^{17}, and 10^{16} cm^{-3} and 2) a semi-transparent 50 cm thick plasma with $n_e = 10^{18}$ cm^{-3}. The total H density (ions plus neutrals) is 10^{12} cm^{-3} in all of the cases at an electron temperature $T_e = 1$ eV. In the semi-transparent case, we need the half-meter thickness to ensure radiation trapping because of the low total H density. The radiation transport is considered along the slab's thickness.

The total amount of H atoms N (cm^{-2}) was "restored" in every case using the SB plot. A comparison of the restored and real values of N for the transparent plasma is shown in Table 1. The SB plot is a straight line in all of the transparent cases with the same slope corresponding to the electron temperature 1 eV. Only the intercept values differ at different n_e values.

In the highest density case, $n_e = 10^{18}$ cm^{-3}, a perfect LTE is established. The 1% relative error reflects the RADTRANSP calculations' accuracy in this case. This error is mostly caused by numerical difficulties due to the photons in the Voigt profile wings. Decreasing n_e violates LTE conditions, which is reflected by an increased relative error. Notice that $n_e = 10^{16}$ cm^{-3} is often considered the critical value when LTE is applicable for H plasma [41,42]. Our results agree with those considerations; however, the relative error caused by violating LTE is noticeably large (30%) at $n_e = 10^{17}$ cm^{-3}.

As noted in Section 2.2, the ratio $A/(n_eC) << 1$ is the quantitative criterion for LTE in the transparent case. This ratio is also presented in Table 1. Its maximum value corresponds to a 6 to 1 transition and defines the error caused by neglecting A_{jk} terms. The values confirm that LTE is established in the 10^{18} cm^{-3} case, but at 10^{16} cm^{-3}, this condition is violated.

We now consider an opaque case with $n_e = 10^{18}$ cm^{-3} and a 50 cm thick slab. As the electron density is very large, LTE is valid for transparent plasma. However, due to the large plasma slab thickness, the Ly-α line is opaque, with an optical thickness of 2.8, while the other lines remain transparent, with an optical thickness < 0.1. (We define the optical thickness in a standard way as $\tau = \int \kappa ds$, where κ is the absorption coefficient and the integral is taken along the ray direction.) It turns out that the Ly-α trapping is sufficient to violate LTE. The population levels become dependent on $\times$,and the line intensities do not fit on a straight line in the SB plot, which is shown in Fig. 1. In this figure, the "real" intensities are indicated by the black markers and the intensities calculated under LTE assumptions are denoted by the red markers connected by the straight line. The lowest levels are affected the most by the plasma opacity. The higher energy levels' populations remain close to the Boltzmann distribution due to large collision rates of the j-k transitions at j and $k \gg 1$.

3.2. Laser pulse with 10^9 W/cm^2 intensity

We now discuss the SB plot technique's precision for LIBS. First, we simulate laser interactions with the target and plasma plume dynamics using the 3DLINE code. The electron density n_e, temperature T_e, and total (ions plus neutrals) H density along a chosen line of sight are found using the calculation results. The reference amount of H is obtained by integrating the H density along the line. Then we use the RADTRANSP code to solve collisional radiative model (CRM) equations with the radiation absorption along the chosen line. The H atom abundances, H ionization degree, and H radiation intensities result from the RADTRANSP calculations. We plot the H intensities on the SB plot to determine the H content along the line of sight. Comparing the total amount of H obtained from the SB plot with the reference value, we find the SB plot technique's relative error.

We modeled interactions of laser radiation with a 1064 nm wavelength with a 10 μm thick W target. The laser beam was directed perpendicularly to the target surface. The pulse duration was 8 ns with a

Table 1
Relative errors of the SB method in a uniform plasma slab. N is the total number of H atoms in the slab.

n_e, cm^{-3}	N from SB, cm^{-2}	Exact N, cm^{-2}	Maximum A/(n_eC)	Relative error, %
10^{18}	4.93 10^7	4.98·10^7	0.08	5
10^{17}	3.30 10^7	4.86·10^7	0.8	32
10^{16}	8.23 10^6	4.66 10^7	8	82

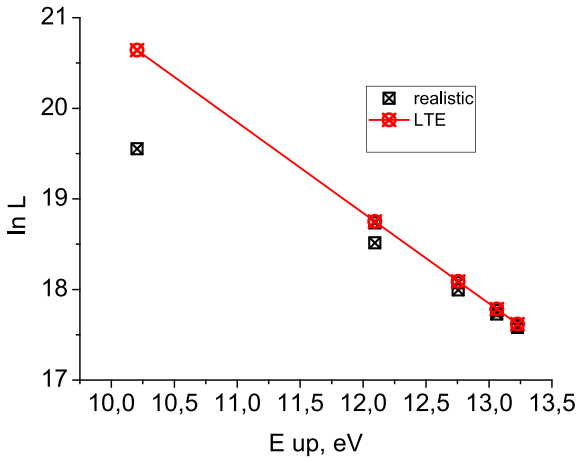

Fig. 1. SB plot of a uniform plasma slab that is opaque at the Ly-α line. The black markers correspond to the intensities of the complete collisional radiative model with radiation transfer. The red markers demonstrate LTE. (For interpretation of the references to colour in this figure legend, the reader is referred to the web version of this article.)

gradual 2 ns increase and decrease in the power as shown in Fig. 2. The pulse energy was 10 mJ, with a radial Gaussian power distribution, a peak intensity of 10^9 W/cm^2, and a beam diameter of 0.5 mm. Thus, the laser spot size on the target was approximately 0.5 mm. These pulse parameters are typically proposed for LIBS for fusion [7].

Since only neutral H density can be determined using the SB plot, the degree of H ionization affects the accuracy of LIBS. Therefore, it is necessary to know the ratio of H^+ to H in the cloud to choose an appropriate observation time. The temporal dependence of the total amount of H and H^+ in the plasma plume derived from the 3DLINE code calculations is plotted in Fig. 3. As discussed in Section 2.1, the total H content (number of H ions plus neutrals in the plume) was calculated as 1% of the W content. The fraction of H^+ ions was determined using the Saha-Boltzmann equation assuming LTE. (The slow growth of the total H content after 50 ns was due to delayed H release from the surface. We did not take into account possible H surface readsorption, which could have reduced or completely eliminated the growth.) Neutral H content dominated after 50 ns. This timescale corresponded to the experimental observations that the H line emission dominated after approximately 100 ns [22]. Before that, continuum radiation prevailed, indicating a large amount of H^+ in the plume.

We used 100, 150, and 200 ns to analyze the SB plot's accuracy. The radiation transport was considered along the $r = 20$ μm chord as illustrated in Fig. 4, in which a 2D map of the electron density n_e is shown at

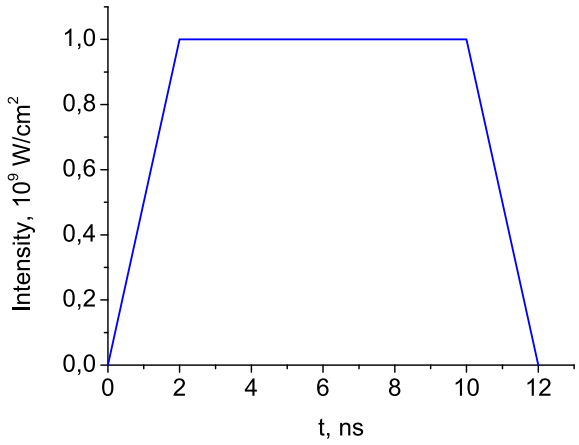

Fig. 2. The laser pulse shape.

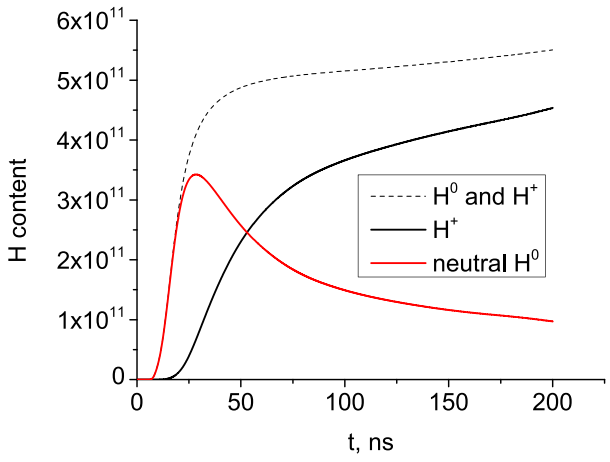

Fig. 3. The total number of H and H^+ particles in the plasma plume in a 10^9 W/cm^2 plasma pulse derived from the 3DLINE calculations. The degree of ionization was calculated using the Saha-Boltzmann equation.

$t = 200$ ns. This chord went through the densest plasma region. The electron temperature and density along the chord are shown in Fig. 5. As the plume cooled down, the density distribution and temperature profiles flattened, but the temperature profiles flattening was much less pronounced.

We now consider the results of RADTRANSP calculations. The H density profiles calculated by RADTRANSP using the full CRM equations with the radiation absorption are shown in Fig. 6. Recall that neither LTE nor radiation transparency were assumed in these calculations. The RADTRANSP input parameters were the electron density n_e given by the W, the total (H plus H^+) hydrogen density, and the temperature. The resulting neutral H density (dashed black curve) at 100 ns was noticeably lower than the total H density (solid black curve) as the degree of ionization was large due to the high T_e. At 200 ns, most of the H was neutralized.

The actual amount of H along the chord was defined by integrating the H neutral density and then comparing the value restored from the SB plot calculated using RADTRANSP. The results are presented in Table 2. The accuracy decreased with the time, and the relative error reached 70% at 200 ns. This tendency agreed with the calculations of the uniform plasma slab presented in Section 3.1. n_e decreased with the time and was closer to the LTE density threshold. The line transparency also decreased. The Ly-α optical thickness changed from 0.8 at 100 ns to 1.0 at 200 ns. This was due to the decreased Stark profile width, which was proportional to n_e. All the other lines remained fully transparent.

Both factors tended to violate LTE conditions and decreased the accuracy. Interestingly, the non-uniform T_e and n_a profiles did not contribute significantly to this error in agreement with Equation , which was satisfied mainly due to strong exponential decay of the density making the right-hand side very large.

The SB plot at 200 ns is shown in Fig. 7. SB plot at 200 ns Fig. 7. The markers correspond to the calculated intensities, the black solid line is the linear fit, and the dashed line is the intensities calculated assuming LTE conditions. The slope of both lines is the same, corresponding to 0.8 eV. The line shift was caused by a deviation from LTE.

The first point at 10.3 eV corresponding to the Ly-α did not fit on the line because of radiation absorption. This point should be discarded when a linear fit is performed. Unfortunately, in some studies, this was not taken into account and the fit was obtained over all of the observed points. Deviations from the straight line were then erroneously interpreted as experimental errors. We emphasize that this is the wrong way to do it. All of the points on the SB plot should not be fit using a single line without considering their opacity. It is also important that all of the points except the Ly-α fit on the straight line even though there is no LTE, meaning that it is impossible to understand whether or not LTE is

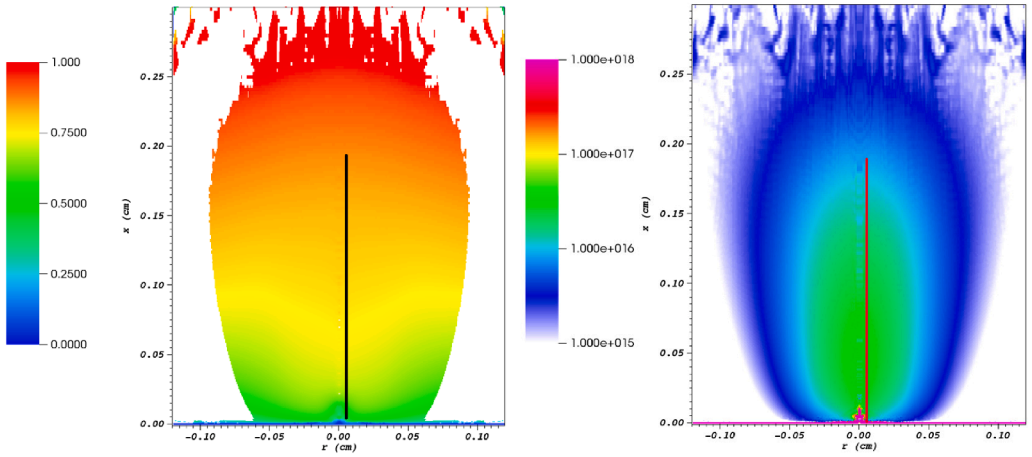

Fig. 4. 2D distribution of the (a) electron temperature and (b) density at 200 ns in a 10^9 W/cm^2 pulse calculated using 3DLINE. RADTRANSP calculations were performed along the red vertical line. (For interpretation of the references to colour in this figure legend, the reader is referred to the web version of this article.)

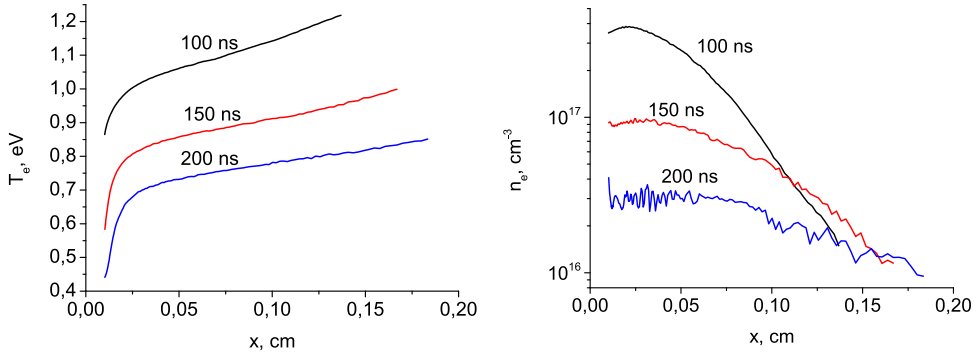

Fig. 5. The electron temperature and density profiles of a 10^9 W/cm^2 laser pulse along the chosen chord (3DLINE results).

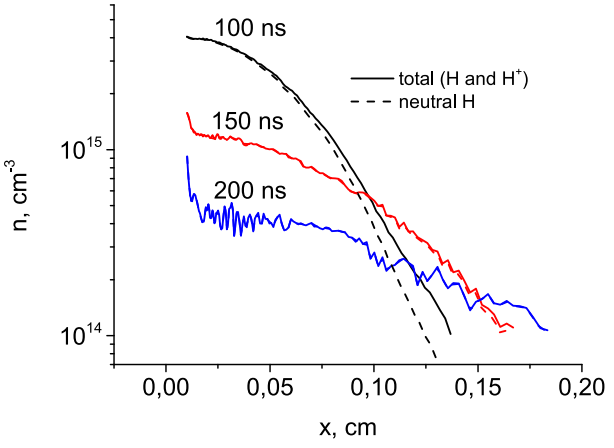

Fig. 6. The H and H^+ densities along the chord in a 10^9 W/cm^2 pulse. The densities were calculated using RADTRANSP with the full collisional radiative model.

established by simply assessing the SB plot.

3.3. Laser pulse with 10^{10} W/cm^2 intensity

We now consider a pulse with a higher intensity of 10^{10} W/cm^2. The other parameters and overall consideration are the same as in the previous section.

The evolution of the H and H^+ content in the cloud is shown in Fig. 8.

Table 2
Relative errors of the SB plot of a 10^9 W/cm^2 pulse at various times. "Exact N" is the integrated number of H atoms along the chosen chord. This number was compared to the number of H atoms along the chord restored from the SB plot. The relative error is shown in the last column.

t, ns	Exact N, cm^{-2}	N from SB, cm^{-2}	Relative error, %
100	$2.1{\cdot}10^{14}$	$1.7{\cdot}10^{14}$	18
150	$1.0{\cdot}10^{14}$	$5.0{\cdot}10^{13}$	51
200	$5.2{\cdot}10^{13}$	$1.6{\cdot}10^{13}$	70

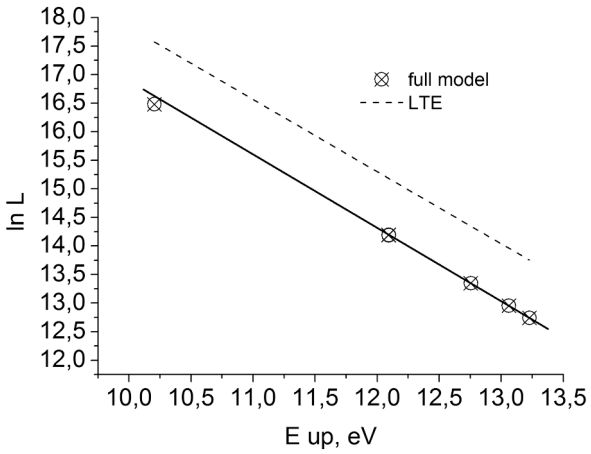

Fig. 7. SB plot at 200 ns in a 10^9 W/cm^2 pulse. LTE is shown by the dashed line.

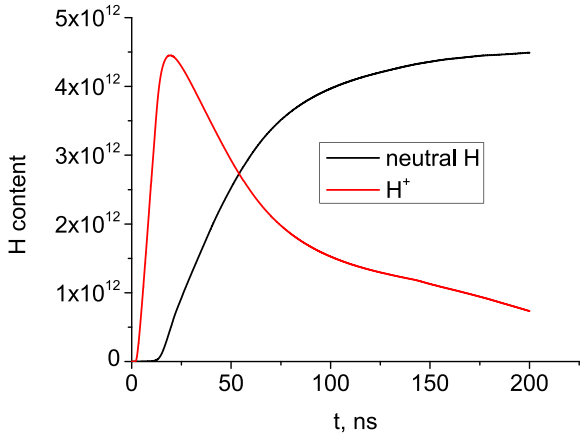

Fig. 8. The total number of H and H^+ particles (3DLINE calculations) in the plasma plume in a 10^{10} W/cm^2 plasma pulse. The degree of ionization was calculated using the Saha-Boltzmann equation.

We used the same times of 100, 150, and 200 ns for the analysis. The ratio of H/H^+ was about the same at 200 ns as it was in the previous case.

The electron temperature and density profiles are plotted in Fig. 9 along the same chord at $r = 20$ μm. Compared to the previous case of 10^9 W/cm^2, n_e tended to be higher, while T_e preserved the same magnitude at $t > 150$ ns. The increase in n_e was expected as the more powerful pulse ablating more W and T_e was large enough to ionize it all.

The LTE conditions were better satisfied at a higher n_e, and the SB plot was more accurate in this case as shown Table 3.

3.4. Pulse intensity of 10^8 W/cm^2

A lower pulse intensity of 10^8 W/cm^2 was also considered. The amount of H and H^+ in the plume is plotted in Fig. 10. In contrast to the previous two cases, the laser intensity was not sufficient to ionize all of the H atoms during the pulse. This may seem favorable for the SB plot technique as neutral H always dominates radiation. Unfortunately, the relative error in this case (Table 4) was the largest. The reason for this was too low n_e in the most radiated regions as shown in Fig. 11. We used different times in this case compared to the previous times to show that the density dynamics fell below the LTE limit. The numerical solution in this case was less stable, especially near the target surface which accounted for the density spikes in Fig. 11. This happened due to the very slow surface ablation caused by the low laser pulse power.

3.5. Discussion

Two main factors define the accuracy of LIBS: the LTE conditions and H degree of ionization. Increasing the electron density leads to deeper

Table 3
The same as in Table 2 but for a 10^{10} W/cm^2 pulse.

t, ns	Exact N, cm^{-2}	N from SB, cm^{-2}	Relative error, %
100	1,1 10^{15}	1,4·10^{15}	−28
150	8,6 10^{14}	6,0·10^{14}	30
200	6,6·10^{14}	4,7·10^{14}	28

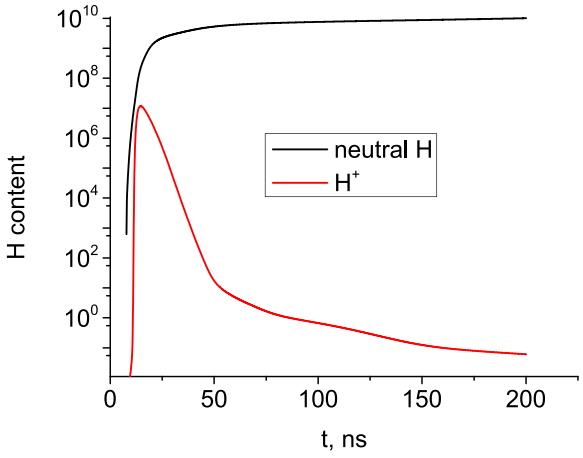

Fig. 10. The total number of H and H^+ particles in the plasma plume in a 10^8 W/cm^2 plasma pulse.

Table 4
The same as in Table 2 but for a 10^8 W/cm^2 pulse.

t, ns	Exact N, cm^{-2}	N from SB, cm^{-2}	Relative error, %
20	1.0·10^{14}	1.9 10^{13}	82
60	7.8 10^{12}	2.9 10^{13}	52
100	9.7·10^{12}	3.25·10^{10}	97

LTE. It also decreases the degree of ionization $\alpha = n[H^+]/(n[H^+] + n[H])$. Indeed, we have from the Saha-Boltzmann equation $\alpha = 1/(1 + K(T_e)n_e)$, where $K = Zexp(E_{ion}/T_e)T_e^{3/2}/K_S$ and K_S is the Saha-Boltzmann constant. Therefore, α increases with the temperature but decreases as the electron density increases. This is due to the dominating role of the three-body recombination, whose rate is proportional to n_e^2, while the electron impact ionization rate $\sim n_e$. Thus, when n_e increases, the recombination grows faster and more H ions recombine. To determine the H content in a sample, n_e is defined by the ionization of the substrate material, in our case W. The electron temperature only weakly depends on the laser pulse power, remaining in a 0.5–1 eV range. n_e increases with the laser power because the amount of ablated W increases. The increase in n_e means that the LTE conditions are better

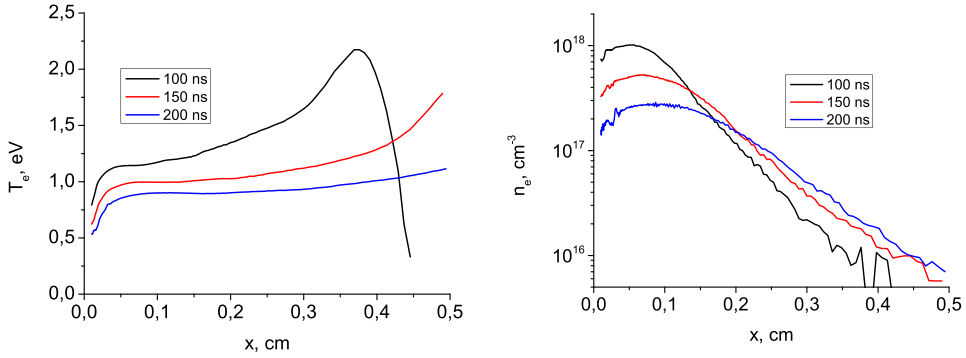

Fig. 9. The electron temperature and density profiles of a 10^{10} W/cm^2 laser pulse along the chosen chord calculated using the 3DLINE code.

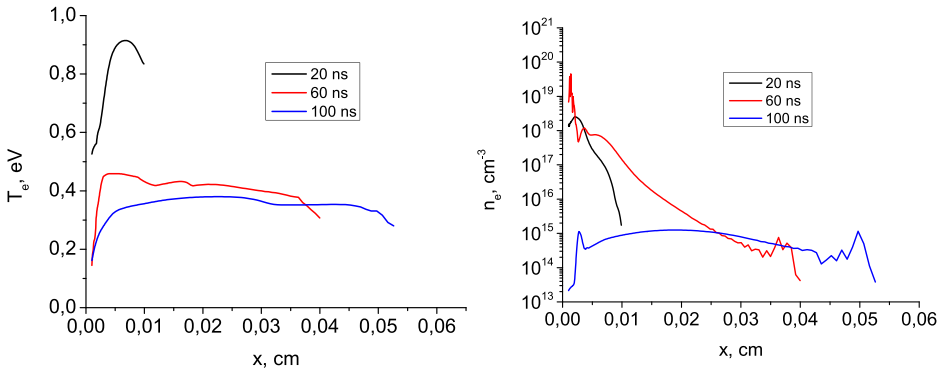

Fig. 11. The electron temperature and density profiles of a 10^8 W/cm^2 laser pulse along the chosen chord.

satisfied and the degree of ionization is smaller. Both factors have a positive impact on the SB plot technique's accuracy. That is why the smallest relative error occurred in the "most powerful" 10^{10} W/cm^2 case.

We stopped our calculations at 200 ns in all of the cases. At 10^{10} W/cm^2 and 10^9 W/cm^2, the H degree of ionization was approximately the same, around 25%. At longer times, n_e decreased and the relative error increased. In practice, the exposure time can be relatively high, longer than 500 ns [22], meaning that integrated intensity is observed, which obviously yields an even higher relative error. Hence, our error estimate was optimistic.

In all of the cases considered, the plasma was optically thick for W radiation. Therefore, it was impossible to use the SB plot to obtain the W content in the plume or estimate the electron density.

In our calculations, we only considered the radiation transport along a chosen line using the backward-forward approximation. In reality, a spectrometer collects emission from the entire plasma plume. However, the chosen chord $r = 20$ μm was in the densest and hottest plasma as shown in Fig. 4, where most of the light emission came from. As the emission along all possible directions registered by the spectrometer integrated, the relative error could not be smaller than that occurring along the considered chord. Therefore, our estimates gave a lower boundary for possible errors.

Some studies suggested that the plasma plume was surrounded by a colder plasma mantle [43,44], at least for LIBS on air. Our simulations demonstrated that at least for LIBS in a vacuum, there is no universal $T_e(x)$ dependence. Indeed, $T_e(x)$ can have a maximum value at the early plume expansion stages (Figs. 9 and 11), increasing monotonously (Fig. 5) or becoming almost flat later (Fig. 11). In the early stages, the maximum value occurs due to laser absorption in a non-uniform plasma plume. Further dynamics of the temperature profile are defined by the complex interplay between two plasma cooling processes: radiation losses depending on the T_e and plasma density, and expansion cooling proportional to the plasma velocity and density.

Our calculations suggest that W and H distributions are coupled by the drag force between them. Although this assumption seems reasonable as discussed in Section 2.1, it is possible that their slight separation could influence the plume's density and temperature distribution. However, we believe that it would not affect our main conclusions but could change the optimal pulse parameters, minimizing the relative errors.

4. Conclusions

We investigated the Saha-Boltzmann (SB) plot's accuracy at determining the H content in a W sample using LIBS. Laser pulses with a 12 ns duration with power densities of 10^8, 10^9, and 10^{10} W/cm^2 were considered. The material ablation and plasma plume dynamics were simulated using the 3DLINE fluid dynamics code. The H radiation was calculated using a collisional-radiative model with the radiation absorption via the RADTRANSP code. Using the H line emission intensities, an SB plot was used to determine the neutral H content in the plume at several times. The calculated values were compared with a nominal amount of H obtained by integrating the known H density. The difference between these numbers demonstrated the relative errors of the SB plot technique.

As a general tendency, we observed that the errors decreased as the laser pulse power increased. The higher the power, the greater the electron density with almost the same electron temperature. A higher n_e provided better LTE conditions and a smaller degree of H ionization. The error in the most typical LIBS pulse parameter, 10^9 W/cm^2, was estimated to be 70% at 200 ns after the pulse and increased over time as the electron density decreased. The 10^8 W/cm^2 pulse doubled the overestimation of the H content in the plasma plume. However, the 10^{10} W/cm^2 pulse had a reasonable error of approximately 30% at 200 ns, which is acceptable to practically assess the H content in fusion reactor materials. Nevertheless, a noticeable amount of H (approximately 20%) was ionized at 200 ns and could not be seen, so one should wait further to determine the total H content as the errors increase over time.

We emphasize that the line intensities of optically thick transitions do not fit on a straight SB line. In our case, the Ly-α line was slightly absorbed. The corresponding intensity should be disregarded when fitting the experimental data. Even if the LTE conditions are violated, the intensities still lie on a straight line in the SB plot, but the intercept values do not correspond to the total amount of H in the plume.

Our estimations seem to be the lower boundary estimate of the relative errors due to the nature of our model. The real errors could be even higher.

Declaration of Competing Interest

The authors declare that they have no known competing financial interests or personal relationships that could have appeared to influence the work reported in this paper.

Acknowledgments

The study was supported by the Ministry of Science and Higher Education of the Russian Federation (project No. 0723-2020-0043).

References

[1] M. Shimada, R.A. Pitts, S. Ciattaglia, S. Carpentier, C.H. Choi, G. Dell Orco, T. Hirai, A. Kukushkin, S. Lisgo, J. Palmer, W. Shu, E. Veshchev, In-vessel dust and tritium control strategy in ITER, J. Nucl. Mater. 438 (2013) S996–S1000.
[2] Roth J, Tsitrone E, Loarer T, Philipps V, Brezinsek S, Loarte A, Counsell G F, Doerner R P, Schmid K, Ogorodnikova O V. and Causey R A 2008 Tritium inventory in ITER plasma-facing materials and tritium removal procedures Plasma Phys. Control. Fusion 50.
[3] G.S. Maurya, A. Marín-Roldán, P. Veis, A.K. Pathak, P. Sen, A review of the LIBS analysis for the plasma-facing components diagnostics, J. Nucl. Mater. 541 (2020) 152417, https://doi.org/10.1016/j.jnucmat.2020.152417.

[4] A. Semerok, C. Grisolia, LIBS for tokamak plasma facing components characterisation: Perspectives on in situ tritium cartography *Nucl. Instruments Methods Phys. Res. Sect. A Accel. Spectrometers*, Detect. Assoc. Equip. 720 (2013) 31–35.

[5] G. Maddaluno, S. Almaviva, L. Caneve, F. Colao, V. Lazic, L. Laguardia, P. Gasior, M. Kubkowska, Detection by LIBS of the deuterium retained in the FTU toroidal limiter *Nucl*, Mater. Energy 18 (2019) 208–211.

[6] F. Colao, S. Almaviva, L. Caneve, G. Maddaluno, T. Fornal, P. Gasior, M. Kubkowska, M. Rosinski, LIBS experiments for quantitative detection of retained fuel *Nucl*, Mater. Energy 12 (2017) 133–138.

[7] B. Schweer, G. Beyene, S. Brezinsek, N. Gierse, A. Huber, F. Irrek, V. Kotov, V. Philipps, U. Samm, M. Zlobinski, Laser techniques implementation for wall surface characterization and conditioning *Phys*, Scr. T T138 (2009) 014008, https://doi.org/10.1088/0031-8949/2009/T138/014008.

[8] G. Cristoforetti, E. Tognoni, L.A. Gizzi, Thermodynamic equilibrium states in laser-induced plasmas: From the general case to laser-induced breakdown spectroscopy plasmas *Spectrochim*, Acta - Part B At. Spectrosc. 90 (2013) 1–22.

[9] G. Cristoforetti, A. De Giacomo, M. Dell'Aglio, S. Legnaioli, E. Tognoni, V. Palleschi, N. Omenetto, Local Thermodynamic Equilibrium in Laser-Induced Breakdown Spectroscopy: Beyond the McWhirter criterion *Spectrochim*, Acta - Part B At. Spectrosc. 65 (1) (2010) 86–95.

[10] J.A. Aguilera, C. Aragón, Multi-element Saha-Boltzmann and Boltzmann plots in laser-induced plasmas *Spectrochim*, Acta - Part B At. Spectrosc. 62 (4) (2007) 378–385.

[11] J.A. Aguilera, C. Aragón, Characterization of a laser-induced plasma by spatially resolved spectroscopy of neutral atom and ion emissions. Comparison of local and spatially integrated measurements *Spectrochim*, Acta - Part B At. Spectrosc. 59 (12) (2004) 1861–1876.

[12] S.M. Zaytsev, A.M. Popov, T.A. Labutin, Stationary model of laser-induced plasma: Critical evaluation and applications *Spectrochim*, Acta - Part B At. Spectrosc. 158 (2019) 105632, https://doi.org/10.1016/j.sab.2019.06.002.

[13] K. Piip, H.J. van der Meiden, K. Bystrov, L. Hämarik, J. Karhunen, M. Aints, M. Laan, P. Paris, H. Seemen, A. Hakola, S. Brezinsek, Loading of deuterium and helium by Pilot-PSI plasma and their detection by in-situ LIBS *Nucl*, Mater. Energy 12 (2017) 694–698.

[14] P. Veis, S. Atikkuke, A. Marin Roldan, V. Dwivedi, M. Veis, P. Barton, M. Jerab, R. Dejarnac, LIBS analysis of samples from the COMPASS vacuum chamber after liquid metal experiments – Li campaign *Nucl*, Mater. Energy 25 (2020) 100809, https://doi.org/10.1016/j.nme.2020.100809.

[15] P. Paris, J. Butikova, M. Laan, A. Hakola, I. Jõgi, J. Likonen, E. Grigore, C. Ruset, Comparison of LIBS results on ITER-relevant samples obtained by nanosecond and picosecond lasers *Nucl*, Mater. Energy 18 (2019) 1–5.

[16] S. Almaviva, L. Caneve, F. Colao, G. Maddaluno, Deuterium detection and quantification by laser-induced breakdown spectroscopy and calibration-free analysis in ITER relevant samples *Fusion Eng*, Des. 146 (2019) 2087–2091.

[17] M. Suchoňová, P. Veis, J. Karhunen, P. Paris, M. Pribula, K. Piip, M. Laan, C. Porosnicu, C. Lungu, A. Hakola, Determination of deuterium depth profiles in fusion-relevant wall materials by nanosecond LIBS *Nucl*, Mater. Energy 12 (2017) 611–616.

[18] S. Almaviva, L. Caneve, F. Colao, G. Maddaluno, N. Krawczyk, A. Czarnecka, P. Gasior, M. Kubkowska, M. Lepek, Measurements of deuterium retention and surface elemental composition with double pulse laser induced breakdown spectroscopy *Phys*, Scr. T167 (2016) 014043, https://doi.org/10.1088/0031-8949/T167/1/014043.

[19] C. Li, D. Zhao, Z. Hu, X. Wu, G.-N. Luo, J. Hu, H. Ding, Characterization of deuterium retention and co-deposition of fuel with lithium on the divertor tile of EAST using laser induced breakdown spectroscopy, J. Nucl. Mater. 463 (2015) 915–918.

[20] C. Li, X. Wu, C. Zhang, H. Ding, G. De Temmerman, H.J. van der Meiden, Study of deuterium retention on lithiated tungsten exposed to high-flux deuterium plasma using laser-induced breakdown spectroscopy *Fusion Eng*, Des. 89 (7-8) (2014) 949–954.

[21] P. Paris, K. Piip, A. Hakola, M. Laan, M. Aints, S. Koivuranta, J. Likonen, A. Lissovski, M. Mayer, R. Neu, V. Rohde, K. Sugiyama, Development of laser induced breakdown spectroscopy for studying erosion, deposition, and fuel retention in ASDEX Upgrade *Fusion Eng*, Des. 98-99 (2015) 1349–1352.

[22] X. Jiang, G. Sergienko, B. Schweer, S. Möller, M. Freisinger, A. Kreter, S. Brezinsek, C.h. Linsmeier, An upgraded LIBS system on linear plasma device PSI-2 for in situ diagnostics of plasma-facing materials *Fusion Eng*, Des. 146 (2019) 96–99.

[23] P. Veis, A. Marín-Roldán, V. Dwivedi, J. Karhunen, P. Paris, I. Jõgi, C. Porosnicu, C. P. Lungu, V. Nemanic, A. Hakola, Quantification of H/D content in Be/W mixtures coatings by CF-LIBS *Phys*, Scr. T171 (2020) 014073, https://doi.org/10.1088/1402-4896/ab7ebd.

[24] Costley A E 2008 Measurement requirements and the diagnostic system on ITER: modifications following the design review 22nd Fusion Energy Conference.

[25] R. Fantoni, S. Almaviva, L. Caneve, F. Colao, A.M. Popov, G. Maddaluno, Development of Calibration-Free Laser-Induced-Breakdown-Spectroscopy based techniques for deposited layers diagnostics on ITER-like tiles *Spectrochim*, Acta - Part B At. Spectrosc. 87 (2013) 153–160.

[26] A.Y. Krukovskiy, V.G. Novikov, I.P. Tsygvintsev, 3D simulation of the impact made by a noncentral laser pulse on a spherical tin target *Math*, Model. Comput. Simulations 9 (1) (2017) 48–59.

[27] I.V. Romanov, I.P. Tsygvintsev, V.L. Paperny, A.A. Kologrivov, Y.V. Korobkin, A. Y. Krukovskiy, A.A. Rupasov, Influence of the laser plasma-expansion specific on a cathode jet formation and the current stability in a laser-ignited vacuum discharge *Phys*, Plasmas 25 (8) (2018) 083107, https://doi.org/10.1063/1.5037001.

[28] Hadjisolomou P, Tsygvintsev I P, Sasorov P, Gasilov V, Korn G and Bulanov S V 2019 Optimisation of Thin Plastic Foil Targets for Production of Laser-Generated Protons in the GeV Range.

[29] B. Iartsev, I. Vichev, I. Tsygvintsev, Y. Sidelnikov, M. Krivokorytov, V. Medvedev, On experimental and numerical study of the dynamics of a liquid metal jet hit by a laser pulse *Exp*, Fluids 61 (2020) 119.

[30] M.M. Basko, I.P. Tsygvintsev, A hybrid model of laser energy deposition for multi-dimensional simulations of plasmas and metals *Comput*, Phys. Commun. 214 (2017) 59–70.

[31] I.Y. Vichev, A.D. Solomyannaya, A.S. Grushin, D.A. Kim, On certain aspects of the THERMOS toolkit for modeling experiments *High Energy Density Phys.* 33 (2019) 100713, https://doi.org/10.1016/j.hedp.2019.100713.

[32] A.J. Kemp, J. Meyer-ter-Vehn, An equation of state code for hot dense matter, based on the QEOS description *Nucl. Instruments Methods Phys. Res. Sect. A Accel. Spectrometers*, Detect. Assoc. Equip. 415 (3) (1998) 674–676.

[33] S. Faik, A. Tauschwitz, I. Iosilevskiy, The equation of state package FEOS for high energy density matter *Comput*, Phys. Commun. 227 (2018) 117–125.

[34] M.M. Basko, Centered rarefaction wave with a liquid-gas phase transition in the approximation of "phase-flip" hydrodynamics *Phys*, Fluids 30 (12) (2018) 123306, https://doi.org/10.1063/1.5064495.

[35] S. Krat, Y.u. Gasparyan, Y.a. Vasina, A. Davletiyarova, A. Pisarev, Tungsten-deuterium co-deposition: Experiment and analytical description *Vacuum* 149 (2018) 23–28.

[36] O.V. Ogorodnikova, Fundamental aspects of deuterium retention in tungsten at high flux plasma exposure, J. Appl. Phys. 118 (7) (2015) 074902, https://doi.org/10.1063/1.4928407.

[37] A.A. Pshenov, A.S. Kukushkin, E.D. Marenkov, S.I. Krasheninnikov, On the role of hydrogen radiation absorption in divertor plasma detachment *Nucl*, Fusion 59 (10) (2019) 106025, https://doi.org/10.1088/1741-4326/ab3144.

[38] E. Marenkov, S. Krasheninnikov, A. Pshenov, Multi-level model of radiation transport in inhomogeneous plasma *Contrib. to*, Plasma Phys. 58 (2018) 570–577.

[39] H.P. Summers, M.G. O'Mullane, Atomic Data and Modelling for Fusion: the ADAS Project *AIP Conf*, Proc. 1344 (2011) 179–187.

[40] M. Leontovich, B. Kadomtsev, Reviews of,, Plasma Physics 12 (1987).

[41] Hans R. Griem, Validity of local thermal equilibrium in plasma spectroscopy *Phys*, Rev. 131 (3) (1963) 1170–1176.

[42] M. Numano, Criteria for local thermodynamic equilibrium distributions of populations of excited atoms in a plasma, J. Quant. Spectrosc. Radiat. Transf. 43 (4) (1990) 311–317.

[43] J. Hermann, A. Lorusso, A. Perrone, F. Strafella, C. Dutouquet, B. Torralba, Simulation of emission spectra from nonuniform reactive laser-induced plasmas *Phys. Rev. E - Stat*, Nonlinear, Soft Matter Phys. 92 (2015) 1–15.

[44] A. Bultel, V. Morel, A. Favre, G. Godard, A. Benyagoub, I. Monnet, A. Sémérok, M. Dinescu, S. Markelj, P. Magaud, C. Grisolia, Towards ps-LIBS tritium measurements in W/Al materials *Fusion Eng*, Des. 146 (2019) 1971–1974.